

## Separation of interface and substrate carrier dynamics at a heterointerface based on coherent phonons

Kunie Ishioka <sup>1,\*</sup> Ethan Angerhofer,<sup>2</sup> Christopher J. Stanton <sup>2</sup> Gerson Mette <sup>3</sup> Kerstin Volz,<sup>3</sup> Wolfgang Stolz,<sup>3</sup> and Ulrich Höfer<sup>3</sup>

<sup>1</sup>*National Institute for Materials Science, Tsukuba 305-0047, Japan*

<sup>2</sup>*Department of Physics, University of Florida, Gainesville, Florida 32611, USA*

<sup>3</sup>*Faculty of Physics and Materials Sciences Center, Philipps-Universität Marburg, 35032 Marburg, Germany*



(Received 10 October 2021; revised 7 January 2022; accepted 7 January 2022; published 26 January 2022)

Transient reflectivity spectroscopy is widely used to study ultrafast carrier and phonon dynamics in semiconductors. In their heterostructures, it is often not straightforward to distinguish contributions to the signal from the various layers. In this work, we perform transient reflectivity measurements on lattice-matched GaP/Si(001) using a near-infrared pulse, to which GaP is transparent. The pump laser pulse can generate coherent longitudinal-optical phonons both in the GaP overlayer as well as in the Si substrate, which have distinct frequencies. This enables us to track the amplitude of the respective signal contributions as a function of the GaP layer thickness  $d$ . The Si phonon signal exhibits a drastic amplitude decrease and a sign change with increasing  $d$ , which can be quantitatively explained by the interference of the probe light reflected at the GaP/Si interface. Based on this knowledge, we can separate the interface contribution and the substrate contribution in the carrier-induced nonoscillatory transient reflectivity signal. The obtained signals reveal interfacial carrier dynamics that is dependent on the GaP layer thickness.

DOI: [10.1103/PhysRevB.105.035309](https://doi.org/10.1103/PhysRevB.105.035309)

### I. INTRODUCTION

Ultrafast carrier and phonon dynamics in semiconductors and their heterostructures can fundamentally influence the performance of electronic devices, and they have therefore been studied extensively using a variety of theoretical and experimental methods [1,2]. Transient reflectivity, a pump/probe technique based on a light-in, light-out detection process, is among the most conventional and widely used experimental methods. It is a particularly powerful technique to detect coherent optical and acoustic phonons, which can be induced by ultrashort laser pulses and detected as periodic modulations of the transient reflectivity at THz and GHz frequencies [3,4]. Because the modulation frequencies are characteristic of the materials, it is relatively straightforward to separate the phonon-induced signals obtained from heterojunctions into contributions from different semiconductor layers. This is not the case for transient reflectivity associated with photoexcited carriers, which typically manifests itself as a superposition of exponential functions. It requires simultaneous measurements of transient reflectivity and a nonlinear optical spectroscopy with surface and interface selectivities, such as second-harmonic generation (SHG), to precisely specify the carrier contributions from specific layers [5].

Among various semiconductor heterostructures, GaAs/AlAs quantum wells and superlattices have been studied most extensively [6–8]. For other combinations of semiconductors, however, lattice mismatch often leads to a strain

at the heterointerface, which can crucially affect the electronic and phononic properties [9–11]. Recently, fabrication of abrupt GaP/Si heterointerfaces without extended defects has been made possible by means of a two-step growth procedure [12–19]. They can also serve as a model heterojunction because of the small lattice mismatch and small intermixing at the interface. In previous studies, systematic transient reflectivity measurements revealed the generation of coherent longitudinal-optical (LO) and longitudinal-acoustic (LA) phonons upon above-band-gap photoexcitation of the GaP layer and the Si substrate [20–22]. The underlying electron-phonon interaction was found to be qualitatively similar to those of the respective bulk semiconductors under the same excitation condition [23,24], except for the reduced LO phonon-plasmon coupling for the thinnest GaP layer examined (thickness  $d = 16$  nm) [22].

By contrast, the GaP/Si interfaces upon below-band-gap excitation of GaP remain mostly unexplored, except for a time-resolved SHG study on a thin ( $d = 4.5$  nm) low-temperature-grown GaP layer [25]. There, a fast ( $< 400$  fs) rise and decay in the SH signal was detected, with its intensity peaked at a pump photon energy of 1.4 eV. In addition, a delayed ( $\sim 2$  ps) rise was observed for pump energies above 1.4 eV. These observations were interpreted as an electronic transition involving a short-lived electronic state at the heterointerface, whose energy lies in the band gaps of the two semiconductors, and the subsequent transport of the photoexcited charge carriers into the Si substrate.

In the present study, we investigate the GaP/Si(001) heterointerfaces with various GaP thicknesses in a pump-probe reflectivity scheme with near-infrared optical pulses. The

\*ishioka.kunie@nims.go.jp

photon energy exceeds the indirect band gap of Si but is well below that of GaP. The reflectivity signals are periodically modulated at the well-resolved frequencies of the LO phonons of GaP and Si, which allows us to separately analyze the phonon signals from the two semiconductors. The amplitude of the Si coherent phonon exhibits an apparently complicated dependence on the GaP overlayer thickness, which can be explained quantitatively by taking into account the interference of the probe wave reflected at the heterointerface. This finding enables us to unambiguously decompose the carrier-induced reflectivity signal into the contributions from the interface and from the substrate.

## II. EXPERIMENTAL METHODS

The samples studied are nominally undoped GaP films grown by metalorganic vapor phase epitaxy with thickness between  $d = 8$  and 48 nm on an exact Si(001) substrate. Details of the fabrication procedure are described elsewhere [14,16]. An 8-nm-thick nucleation layer of GaP is first grown in a flow-rate modulated epitaxy at 450 °C for all the samples studied. The as-grown GaP nucleation layer consists of crystalline grains with a lateral size of  $\lesssim 30$  nm [14]. To grow thicker ( $d = 18$ –48 nm) GaP layers, the GaP layer is overgrown in a continuous epitaxy at 675 °C. This two-step growth procedure minimizes the density of planar defects and enhances self-annihilation of antiphase domains, leading to an abrupt GaP/Si interface, as shown schematically in Fig. 1(a) [15,17]. We note that the maximum GaP thickness in the present study is well below the critical layer thickness ( $d \simeq 70$  nm), above which the GaP crystallinity is degraded because of the slightly different equilibrium lattice constants between GaP and Si [14].

Single-color pump-probe reflectivity measurements are performed in ambient conditions in a near-backreflection geometry. To investigate the phonon dynamics, an output of a Ti:sapphire oscillator with 12-fs duration, 815-nm center wavelength, and 80-MHz repetition rate is used as the light source. GaP is transparent to the 815-nm light, whereas the optical penetration depth in Si is  $\sim 10$   $\mu\text{m}$  [26]. A spherical mirror brings the linearly polarized pump and probe beams to a  $\sim 30$ - $\mu\text{m}$ -diam spot on the sample with incident angles of  $\lesssim 15^\circ$  and  $\lesssim 5^\circ$  from the surface normal. Anisotropy in the pump-induced reflectivity change,  $\Delta R_{\text{eo}} \equiv \Delta R_H - \Delta R_V$ , is measured by detecting the horizontal ( $H$ ) and vertical ( $V$ ) polarization components of the probe light with a pair of matched photodiode detectors, as shown in Fig. 1(b). This scheme is suitable to detect the LO phonons of GaP and Si, which have only off-diagonal Raman tensor components as described by Eq. (A3) in Appendix A, but it is not ideal to monitor the mostly isotropic carrier dynamics. The signal from the detector pair is preamplified and is averaged in a digital oscilloscope typically over 10 000 times while the delay  $t$  between the pump and probe pulses is scanned continuously with a fast scan delay.

To examine the carrier dynamics, an output of a regenerative amplifier with 150 fs duration, 810 nm wavelength, and 100 kHz repetition rate is used as the light source. The pump and probe spot size on the sample is  $\sim 100$   $\mu\text{m}$ . Pump light is chopped at a frequency of  $\sim 2$  kHz for lock-in detection.

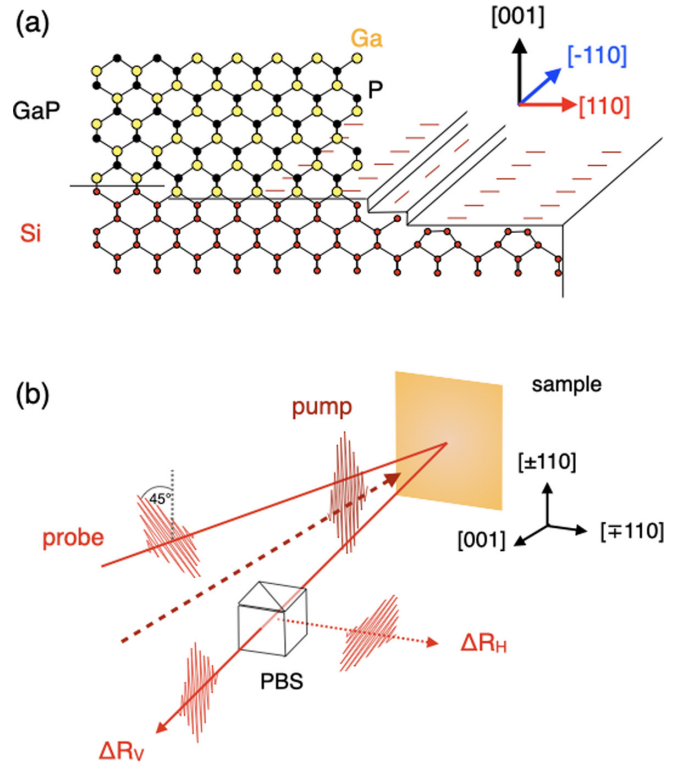


FIG. 1. (a) Model of the GaP/Si(001) interface [16]. Red, yellow, and black circles represent silicon, gallium, and phosphorus atoms, respectively. (b) Schematic illustration of the configuration for the anisotropic reflectivity detection. PBS denotes polarizing beam splitter cube.

Pump-induced change in the reflectivity  $\Delta R$  is measured by detecting the probe lights before and after the reflection with a pair of matched photodiode detectors. The signal from the detector pair is amplified with a current preamplifier and a lock-in amplifier. The time delay  $t$  between the pump and probe pulses is scanned with a linear motor stage (slow scan).

## III. RESULTS

### A. LO phonon dynamics

We first examine the phonon dynamics by measuring  $\Delta R_{\text{eo}}/R_0$  using a 12-fs laser pulse at an incident pump fluence of 0.18  $\text{mJ}/\text{cm}^2$ . Figure 2(a) shows a typical anisotropic reflectivity change for the  $d = 48$  nm GaP/Si sample. We extract its oscillatory part by subtracting the nonoscillatory baseline that can be fitted to a multiple exponential function. The obtained oscillations are summarized in Fig. 2(b) for all the GaP/Si samples at two representative pump polarizations. The oscillations consist mainly of two frequencies, 12 and 15.6 THz, which are seen as sharp peaks in the fast-Fourier-transformed (FFT) spectra in Fig. 2(c). These peaks arise from coherent LO phonons of GaP and Si, respectively, as is evident from the comparison with the signals of bulk GaP and Si shown in the same figure [27].

For the bulk GaP and Si crystals, the  $[-110]$  and  $[110]$  crystallographic directions are equivalent. Correspondingly, the LO phonon amplitudes are comparable between the pump polarizations along these two directions, as shown in

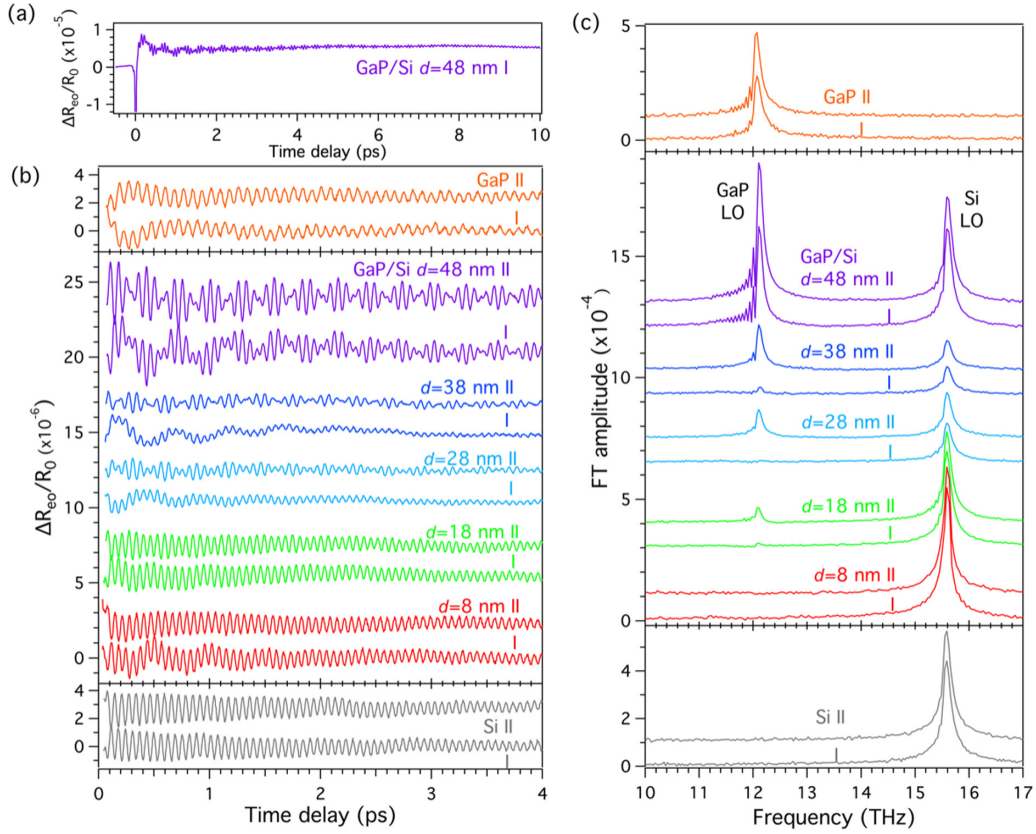


FIG. 2. (a) Anisotropic reflectivity change for  $d = 48$  nm. (b) Oscillatory parts of the anisotropic reflectivity changes of GaP/Si(001) samples with different  $d$ . (c) Fast Fourier transform spectra of (b) in the optical phonon regime. Pump polarization is either parallel to the  $[-110]$  or  $[110]$  directions of the Si substrate (labeled, respectively, with I and II). Probe light is polarized nearly along the  $[100]$  direction for the anisotropic detection. Reflectivity signals from (001)-oriented Si and GaP wafers are also shown for comparison. Incident pump density is  $0.18$  mJ/cm<sup>2</sup>. Traces are offset for clarity.

Figs. 2(b) and 2(c), while the phases of the oscillations are opposite to each other because of the Raman generation, as explained in Appendix A. For the GaP/Si samples, by contrast, the two directions can be distinguished based on the miscut of the Si substrate surface, as schematically shown in Fig. 1(a). The GaP peak height in Fig. 2(c) is apparently larger for pump polarization along the  $[110]$  axis (labeled “II”) than along the  $[-110]$  axis (“I”). For a fixed pump polarization, the GaP peak height increases monotonically with increasing  $d$ . By contrast, the Si peak height is comparable between the two polarizations for all the GaP/Si samples examined. It depends on  $d$  in an apparently complicated manner, however, i.e., first it decreases and then it increases with increasing  $d$ .

For quantitative analyses, we fit the oscillatory signals to a multiple damped harmonic function:

$$f(t) = \sum_i A_i \exp(-\Gamma_i t) \sin(2\pi \nu_i t + \phi_i), \quad (1)$$

with  $i$  denoting different phonon modes. Figure 3 compares the experimentally obtained oscillations with the fits and their GaP and Si phonon components at a fixed pump and probe polarization combination. Whereas the GaP oscillation component simply increases in the amplitude with increasing  $d$ , the Si component flips its phase between  $d = 38$  and  $48$  nm. We note that the frequencies  $\nu_i$  and the dephasing rates  $\Gamma_i$  show no systematic dependence on the GaP thickness  $d$ , and

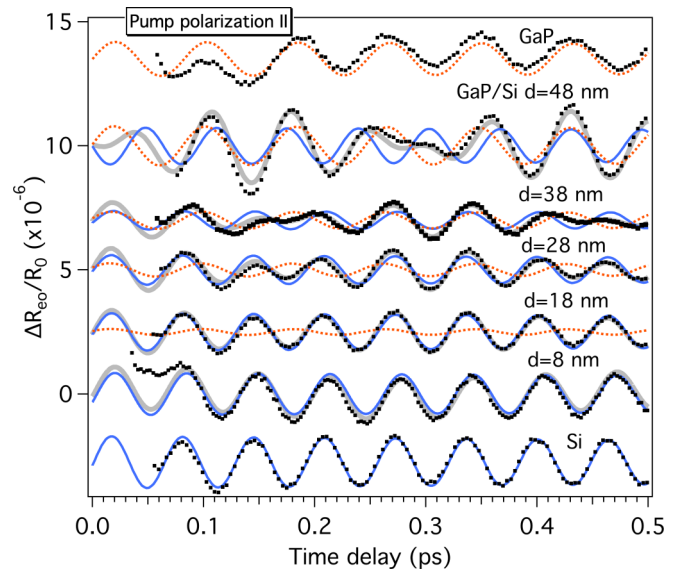


FIG. 3. Comparison of oscillatory parts of  $\Delta R_{\text{eo}}/R_0$  obtained at pump polarization II (black dots) with fits to Eq. (1) (gray curves). Blue solid and orange dotted curves represent the fit components of Si and GaP LO phonons, respectively. Signals and fits for the bulk Si and GaP are also shown for comparison. Traces are offset for clarity.

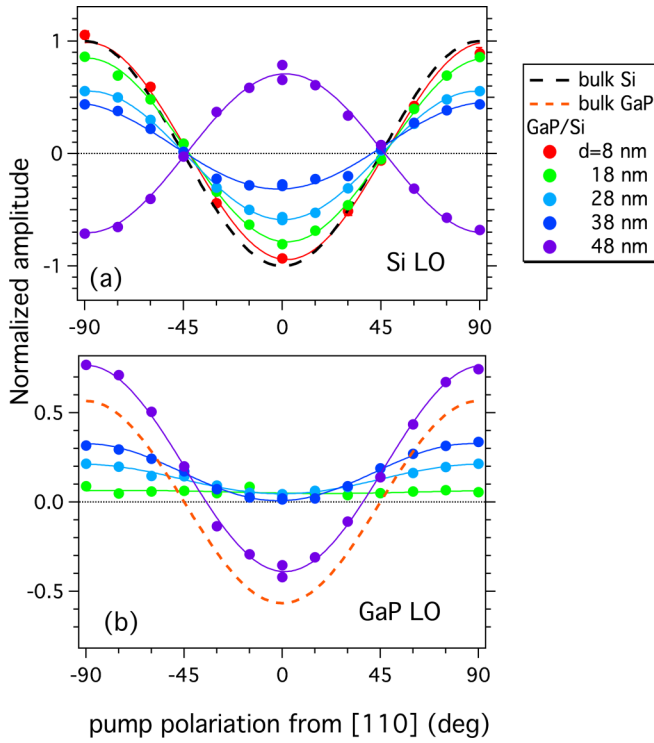


FIG. 4. LO phonon amplitudes  $A_{\text{Si}}$  (a) and  $A_{\text{GaP}}$  (b) of the GaP/Si samples as a function of pump polarization angle  $\theta$  from the [110] direction of the Si substrate. Vertical axes are normalized by  $A_{\text{Si}}$  of bulk Si at  $\theta = 90^\circ$ . Solid curves represent the fits to Eqs. (2) and (3). Amplitudes for the bulk Si and GaP are also shown with broken curves for comparison.

they agree with those of the bulk GaP and Si within experimental errors.

Figure 4 plots the GaP and Si phonon amplitudes,  $A_{\text{GaP}}$  and  $A_{\text{Si}}$ , as a function of pump polarization angle  $\theta$  from the [110] axis of the Si substrate. Here we restrict the initial phase  $\phi_i$  around zero and allow  $A_i$  to take a positive or negative value to represent the phase flip. The Si phonon amplitude [Fig. 4(a)] always follows a cosine function of  $\theta$ :

$$A_{\text{Si}}(d, \theta) = -B_{\text{Si}}(d) \cos 2\theta \quad (2)$$

for all the GaP/Si samples as well as for the bulk Si. This is an evidence of the generation of coherent LO phonons via impulsive stimulated Raman scattering (ISRS), as described by Eq. (A4) in Appendix A. The GaP phonon amplitude for the *bulk* GaP, plotted with an orange broken curve in Fig. 4(b), shows a similar  $\theta$ -dependence, indicating an ISRS generation in the present below-band-gap excitation condition [24].

The GaP phonon amplitude for the GaP/Si samples, by contrast, is described more appropriately with an additional  $\theta$ -independent term by

$$A_{\text{GaP}}(d, \theta) = C_{\text{GaP}}(d) - B_{\text{GaP}}(d) \cos 2\theta. \quad (3)$$

A similar  $\theta$ -independent component was also observed for *bulk* GaP upon above-band-gap photoexcitation with 3-eV light, and it was attributed to the coherent phonon generation via ultrafast screening of the built-in dc field in the surface depletion region by photoexcited carriers [24]. The driving force for this transient depletion field screening (TDFS) mechanism

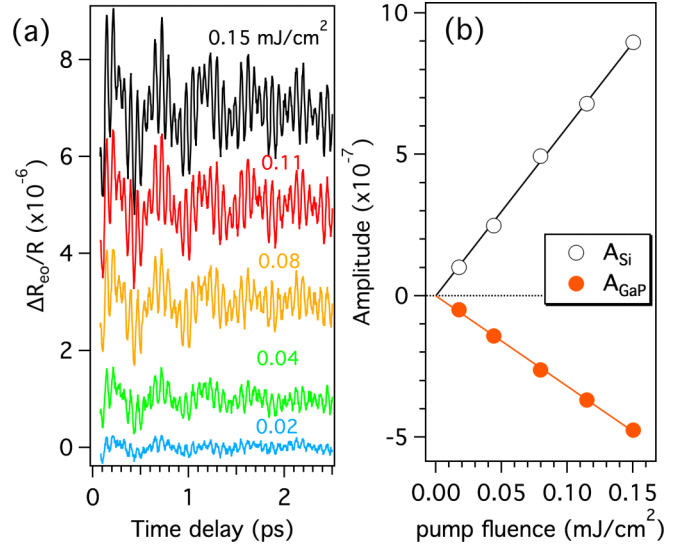


FIG. 5. (a) Oscillatory part of the anisotropic reflectivity change of  $d = 48$  nm GaP/Si pumped at different incident fluences. Pump polarization is parallel to the [110] direction of the Si substrate. Traces are offset for clarity. (b) Pump fluence dependences of the LO phonon amplitudes, obtained by fitting the traces in (a) to Eq. (1). Lines represent linear fits.

is independent of the pump polarization for a cubic crystal such as GaP, as described by Eq. (A5) in Appendix A. In the present study, we similarly attribute the  $\theta$ -independent term  $C_{\text{GaP}}$  of the GaP/Si samples to the TDFS-driven LO phonons.

The coherent phonon generation via TDFS would require a photoinduced ultrafast current in a polar semiconductor, as described in Appendix A. Carrier creation via linear absorption is unlikely for the present pump photon energy (1.5 eV), however, because it is well below the indirect band gap of GaP (2.3 eV). Two-photon absorption (TPA) is not likely to dominate the photoexcitation either, for the following reasons. First, the phonon amplitude  $A_{\text{GaP}}$  increases linearly with increasing pump fluence for all the GaP/Si samples examined, as shown in Fig. 5 for  $d = 48$  nm, for example, demonstrating that the coherent phonon generation is predominantly a one-photon process. Secondly, the carrier density created via TPA in (bulk) GaP under the present excitation condition is estimated to be  $\lesssim 10^{16} \text{ cm}^{-3}$ , and the corresponding change in the transient reflectivity is estimated to be  $\Delta R/R_0 \lesssim 10^{-6}$ , as described in Appendix B. The latter is smaller than the experiment by at least an order of magnitude [28]. A more likely source of the charge carriers in the GaP layer would be via injection at the GaP/Si interface, either from the interface electronic states reported in the previous SHG study [25] or from the Si substrate, as we will discuss further in Sec. IV B.

Figure 6 summarizes the  $d$ -dependence of the amplitude components  $B_i$  and  $C_i$  obtained from fitting  $A_i(\theta)$  to Eq. (3). The components  $B_{\text{GaP}}$  and  $C_{\text{GaP}}$  increase in parallel with increasing  $d$  up to 38 nm. At  $d = 48$  nm,  $B_{\text{GaP}}$  becomes several times larger than  $C_{\text{GaP}}$ , indicating that the bulklike ISRS overwhelms the interface-specific TDFS of the thickest GaP layer. By contrast, the component for the Si LO mode,  $B_{\text{Si}}$ , decreases almost monotonically with increasing  $d$  up to 38 nm. At  $d = 48$  nm it takes a negative value, denoting a phase flip

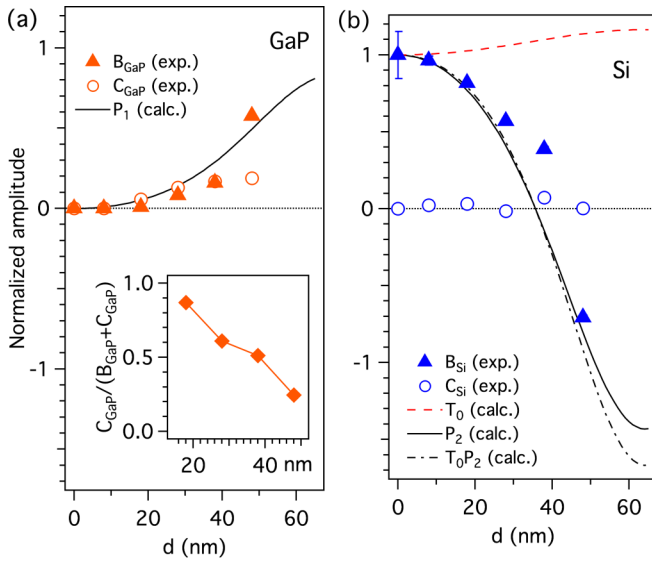


FIG. 6.  $\theta$ -dependent ( $B$ , filled triangles) and  $\theta$ -independent ( $C$ , empty circles) amplitude components of GaP (a) and Si (b) LO phonons, as a function of GaP layer thickness  $d$ . The components are normalized by  $B_{\text{Si}}$  of bulk Si ( $d = 0$  nm). Solid curves in (a) and (b) represent  $P_1$  and  $P_2$  calculated with Eqs. (9) and (10). Red broken and black chain curves in (b) represent  $T_0$  given by Eq. (5) and  $T_0P_2$ , respectively.  $P_1$  and  $P_2$  are normalized by  $P_2$  ( $d = 0$ ), whereas  $T_0$  is normalized by  $T_0$  ( $d = 0$ ). The inset in (a) plots the amplitude component ratio  $C_{\text{GaP}}/(B_{\text{GaP}} + C_{\text{GaP}})$  as a function of  $d$ .

of the coherent oscillation. We will discuss the origin of this peculiar behavior in Sec. IV A.

### B. Carrier dynamics

To examine the carrier dynamics that can possibly contribute to the TDFS, we also measure the transient reflectivity  $\Delta R/R_0$  using a 150-fs laser pulse at an incident pump fluence of  $0.25 \text{ mJ/cm}^2$ . Gray curves in Fig. 7(a) compare the as-measured reflectivity changes of the GaP/Si samples with that of bulk Si. The signal from the bulk Si shows a step-function-like drop at  $t = 0$ , followed by very small recovery in the present time window. The response is in good agreement with previous reports [29,30] and can be attributed to the free-carrier excitation across the indirect band gap, followed by their diffusion and recombination at the surface. Bulk GaP, by contrast, exhibits no detectable change under the present photoexcitation condition and its signal is therefore not shown. This gives additional evidence that TPA in GaP is negligible in the present study.

Transient reflectivity traces of the GaP/Si samples are qualitatively different from those of the bulk Si and GaP, indicating the carrier dynamics that is characteristic to the GaP/Si heterointerface. For  $d = 8$  nm, the reflectivity signal shows an abrupt drop at  $t \simeq 0$  that is somewhat similar to the bulk Si, though the subsequent recovery is more distinct. The signals from the thicker ( $d \geq 18$  nm) GaP/Si, by contrast, show an initial abrupt drop or rise depending on  $d$ , followed by a subpicosecond increase and then a slower decrease. The height of the initial abrupt drop or rise, which we represent with the transient reflectivity at  $t = 0.5$  ps, exhibits a peculiar

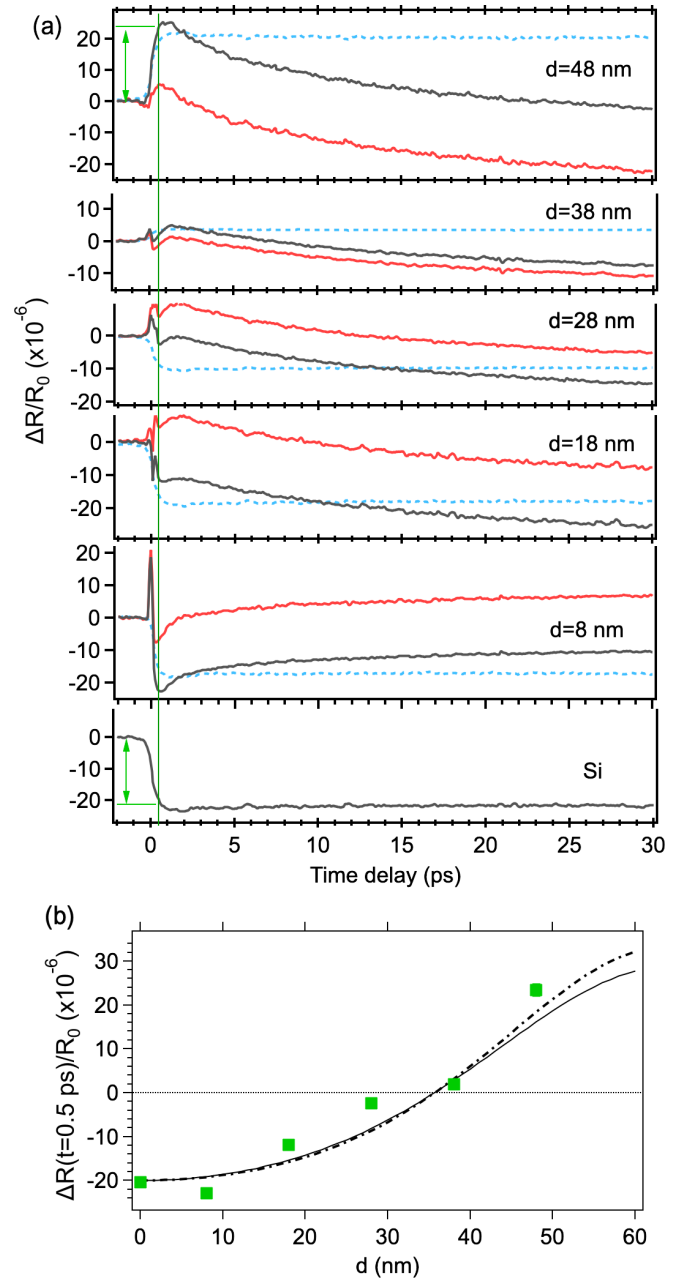


FIG. 7. (a) As-measured transient reflectivity signals  $\Delta R/R_0$  (gray curves) of GaP/Si(001) and bulk Si. Pump and probe lights are polarized along the [110] axes of the Si substrate. Incident pump density is  $0.25 \text{ mJ/cm}^2$ . The vertical line indicates  $t = 0.5$  ps, and arrows indicate the initial step height  $\Delta R(t = 0.5 \text{ ps})/R_0$  for selected traces. Blue broken and red solid curves indicate the contributions from the substrate and the interface given by Eqs. (11) and (12). (b) Initial step height  $\Delta R(t = 0.5 \text{ ps})/R_0$  as a function of GaP layer thickness  $d$  (filled squares). Solid and chain curves represent the  $d$ -dependence of  $P_2$  and  $T_0P_2$ . Curves are scaled to  $\Delta R(t = 0.5 \text{ ps})/R_0$  of bulk Si.

$d$ -dependence, as shown in Fig. 7(b). It starts from a negative value and increases monotonically with increasing  $d$  until it reaches a positive value. This trend is very similar to that of the Si LO phonon amplitude,  $B_{\text{Si}}$ , if we normalize the initial step height by that of the bulk Si.

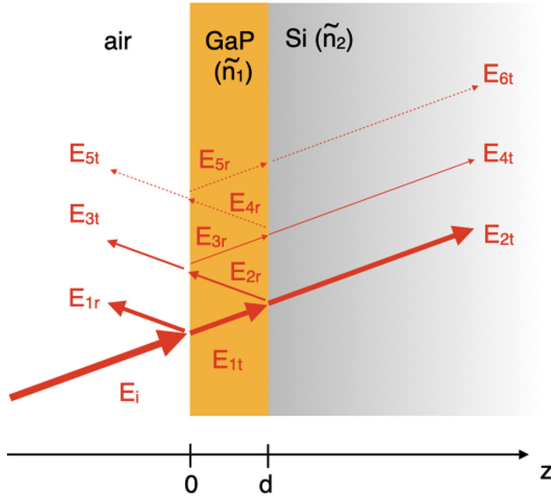


FIG. 8. Schematic illustration of the transmission and reflection of probe electric field that is incident on a GaP/Si interface.  $E_i$ : incident wave;  $E_{jr}$  and  $E_{jt}$ : reflected and transmitted wave at the  $j$ th interface. Incidence angle is exaggerated for clarity.

#### IV. DISCUSSION

##### A. $d$ -dependence of the substrate contribution to the transient reflectivity signal

In the previous section, we have seen that the phonon- and the carrier-induced signals from the Si substrate exhibit similar overlayer thickness dependences. In this subsection, we theoretically model the effect of the GaP overlayer on the pump-induced reflectivity signal from the buried Si substrate by explicitly taking into account the light carrier wave.

We first examine the effect of the GaP overlayer on the pump light incoming to the Si substrate, whose details are described in Appendix C. We assume a light pulse, whose electric field in air is described by

$$E_i(z, t) = \tilde{E}_i(z, t)e^{i(k_0z - \omega_0 t)}, \quad (4)$$

being incident on a GaP/Si heterointerface from the normal direction. At the air/GaP ( $z = 0$ ) and GaP/Si ( $z = d$ ) interfaces, the light pulse is partially reflected and partially transmitted, as schematically shown in Fig. 8. Taking into account the multiple reflections, the transmittance of the heterointerface, or the intensity ratio of the light penetrating into Si to the incident light, can be expressed by

$$T_0(d) = \frac{(1 - r_{01}^2)(1 - r_{12}^2)}{1 + r_{01}^2 r_{12}^2 + 2r_{01} r_{12} \cos 2n_1 k_0 d}, \quad (5)$$

with

$$r_{01} \equiv \frac{\tilde{E}_{1r}}{\tilde{E}_i} = \frac{1 - n_1}{1 + n_1},$$

$$r_{12} = \frac{\tilde{E}_{2r}}{\tilde{E}_{1t}} = \frac{n_1 - n_2}{n_1 + n_2} \quad (6)$$

representing the reflection coefficients for the light wave coming from air into GaP and from GaP into Si, respectively.  $n_1$  and  $n_2$  are the refractive indices of GaP and Si.

Equation (5) implies that the pump intensity in the Si substrate can depend on the overlayer thickness  $d$  due to the interference among different optical paths ( $E_{2t}$ ,  $E_{4t}$ ,  $E_{6t}$ , ... in Fig. 8). This is the same principle as used for antireflection coatings on optics surfaces. In the present case of GaP/Si, however, the contribution from the  $d$ -dependent term is insignificant, because  $r_{12}$  is small as a consequence of comparable refractive indices of GaP ( $n_1 = 3.18$ ) and Si ( $n_2 = 3.68$ ). The pump intensity in Si is modified no more than 15% by varying  $d$ , as shown with a red broken curve in Fig. 6(b), which by itself cannot explain the drastic thickness dependence of the Si phonon and carrier signals observed in our experiments.

Next we examine the effect of the GaP overlayer on the probe light, the details of which are described in Appendix D. The overlayer similarly modifies the reflectance as a function of film thickness  $d$ :

$$R_0(d) = \frac{r_{01}^2 + r_{12}^2 + 2r_{01}r_{12} \cos 2n_1 k_0 d}{1 + r_{01}^2 r_{12}^2 + 2r_{01}r_{12} \cos 2n_1 k_0 d}. \quad (7)$$

We assume that a separate pump pulse induces small disturbances  $\delta n_1(z, t)$  and  $\delta n_2(z, t)$  in the refractive indices of the GaP layer and the Si substrate. Coherent phonons in the respective semiconductors modulate the refractive indices periodically as a function of  $t$ , whereas photoexcited carriers in Si induce a step-function-like change in  $n_2$ . In either case, the transient reflectivity can be expressed by taking its derivatives with respect to the refractive indices:

$$\frac{\Delta R}{R_0} = \frac{1}{R_0} \left( \frac{\partial R_0}{\partial n_1} \delta n_1 + \frac{\partial R_0}{\partial n_2} \delta n_2 \right) \equiv P_1 \delta n_1 + P_2 \delta n_2. \quad (8)$$

The first and second terms of Eq. (8) represent the pump-induced reflectivity changes contributed by the GaP overlayer and by the Si substrate. They can be given, respectively, by

$$P_1(d) \delta n_1 = \frac{1}{R_0} \left( \frac{\partial R_0}{\partial r_{01}} \frac{\partial r_{01}}{\partial n_1} + \frac{\partial R_0}{\partial r_{12}} \frac{\partial r_{12}}{\partial n_1} + \frac{\partial R_0}{\partial (n_1 k_0 d)} \frac{\partial (n_1 k_0 d)}{\partial n_1} \right) \delta n_1$$

$$= \frac{2(r_{01}^2 - 1)(1 - r_{12}^2)}{(r_{01}^2 + r_{12}^2 + 2r_{01}r_{12} \cos 2n_1 k_0 d)(1 + r_{01}^2 r_{12}^2 + 2r_{01}r_{12} \cos 2n_1 k_0 d)}$$

$$\times \left[ \frac{r_{01}(1 + r_{12}^2) - r_{12}(1 + r_{01}^2)}{2n_1} (1 - \cos 2n_1 k_0 d) + 2k_0 d r_{01} r_{12} \sin 2n_1 k_0 d \right] \delta n_1, \quad (9)$$

$$P_2(d) \delta n_2 = \frac{1}{R_0} \frac{\partial R_0}{\partial r_{12}} \frac{\partial r_{12}}{\partial n_2} \delta n_2 = \frac{2r_{12}(1 - r_{01}^4) + 2r_{01}(1 + r_{12}^2)(1 - r_{01}^2) \cos 2(n_1 k_0 d)}{(r_{01}^2 + r_{12}^2 + 2r_{01}r_{12} \cos 2n_1 k_0 d)(1 + r_{01}^2 r_{12}^2 + 2r_{01}r_{12} \cos 2n_1 k_0 d)} \frac{-2n_1}{(n_1 + n_2)^2} \delta n_2. \quad (10)$$

Solid curves in Fig. 6 show the  $d$ -dependences of the pump-induced reflectivity changes given by Eqs. (9) and (10). The calculations reasonably reproduce the experimentally obtained Si and GaP phonon signals,  $B_{\text{Si}}$  and  $B_{\text{GaP}}$ , of the GaP/Si samples. Equation (10) also reproduces the  $d$ -dependence of the initial step height,  $\Delta R(t = 0.5\text{ps})/R_0$ , as shown in Fig. 7(b), indicating that the initial drop/rise arise mostly (but not entirely) from the photoexcitation in the Si substrate. Taking into account the  $d$ -dependence of the pump intensity [Eq. (5)] introduces only a minor correction, as shown with chain curves in Figs. 6(b) and 7(b). The agreements confirm that the interference effect on the reflected *probe* light is the origin of the oscillatory behavior of the transient reflectivity signal from the Si substrate, whether it is associated with phonons or carriers.

### B. Extraction and interpretation of interface contributions to transient reflectivity

We can now use Eq. (10) to decompose the carrier-induced signal into the substrate and interface contributions. We can express the Si substrate contribution with

$$\frac{\Delta R_{\text{sub}}(t, d)}{R_0} = \frac{T_0(d)P_2(d)}{T_0(0)P_2(0)} \frac{\Delta R_{\text{Si}}(t)}{R_0}, \quad (11)$$

where  $\Delta R_{\text{Si}}(t)/R_0$  represents the transient reflectivity signal of the bulk Si obtained under the same condition. The contribution from the interface is then given by

$$\frac{\Delta R_{\text{int}}(t, d)}{R_0} = \frac{\Delta R(t, d)}{R_0} - \frac{\Delta R_{\text{sub}}(t, d)}{R_0}. \quad (12)$$

The substrate and interface contributions given by Eqs. (11) and (12) are shown in Fig. 7(a) with blue broken and red solid curves, respectively.

The obtained interface contribution is qualitatively different between the nucleation layer ( $d = 8$  nm) and the overgrown layers ( $d = 18$ – $48$  nm). For  $d = 8$  nm, it exhibits an abrupt drop to  $\Delta R_{\text{int}}/R_0 \lesssim -10^{-5}$  at  $t = 0$ , followed by a biexponential increase with time constants  $\tau_{\text{fast}} = 1.6$  ps and  $\tau_{\text{slow}} = 43$  ps toward a positive value. For GaP, the reflectivity change of  $10^{-5}$  would correspond to the photoexcited carrier density of  $\sim 10^{17}$  cm $^{-3}$ , as described in Appendix B. This is a few orders of magnitude higher than the carrier density that would be created via TPA [Eq. (B4) in Appendix B], and therefore excludes TPA as the dominant excitation path. The fast time constant for the following recovery is close to the delayed rise time reported in the previous SHG study on a 4.8-nm-thick GaP/Si [25], which was associated with carrier injection from the interface electronic state into the Si substrate. The slow time constant is comparable to that of bulk Si, 38 ps, and it can be interpreted in the similar relaxation processes involving the carrier diffusion within the Si substrate and their recombination at the GaP/Si interface. The amplitude of the slow relaxation is larger than for bulk Si indicating a higher density of the recombination centers at the GaP/Si heterointerface than at the naturally oxidized surface of bulk Si.

For the overgrown GaP layers ( $d = 18$ – $48$  nm), the interface contribution *rises*, instead of drops, to  $\Delta R_{\text{int}}/R_0 \lesssim 10^{-5}$  within a picosecond, followed by a monotonic decrease on

a  $\sim 30$  ps timescale. The qualitative difference in the early-time response suggests a different excitation path from that of the nucleation layer ( $d = 8$  nm). Again, TPA in GaP can be excluded based on the rise height. We consider the interface signals for the overgrown layers to be contributed, at least partially, by carrier injection into the GaP overlayer, based on the deviation of the polarization dependence of the GaP LO phonons from that of bulk GaP (Fig. 4). The timescale of the slow decrease,  $\sim 30$  ps, is independent of  $d$  and comparable to those for  $d = 8$  nm GaP/Si and bulk Si, suggesting a similar recombination process at the heterointerface.

The TDFS generation of the coherent LO phonons would require the rise time of the driving force, which is given by the drift-diffusion current described by Eq. (A5) in Appendix A, to be shorter than half the phonon period ( $\sim 50$  fs). This does not necessarily mean that the carriers injected at the heterointerface need to be transported to the GaP/air surface within 50 fs. The drift-diffusion current is typically created by photocarriers being accelerated by a built-in dc field within a surface (or interface) depletion region. The TDFS generation would therefore occur most efficiently in the vicinity of the GaP/Si interface, where the dc field is strongest and where the drift current arrives fast enough. This spatial inhomogeneity explains why the TDFS is dominant for the relatively thin overgrown layer [ $C_{\text{GaP}}/(B_{\text{GaP}} + C_{\text{GaP}}) = 0.87$  at  $d = 18$  nm], but its contribution becomes smaller with increasing  $d$  (0.25 at  $d = 48$  nm), as shown in the inset of Fig. 6(a).

We note that the dominant source for the carrier injection into the overgrown GaP layer cannot be determined conclusively by the present study alone. On the one hand, the pump photon energy in the present study is not far from that of the interface resonance (1.4 eV) reported for a thin GaP nucleation layer in the previous SHG study [25]. One might therefore expect that carriers could be injected from the interface states. On the other hand, the qualitatively different response in  $\Delta R_{\text{int}}/R_0$  between the nucleation layer and the overgrown layers can be an indication of a different excitation path. Previous theoretical and experimental studies on (001)-oriented Si/GaP interfaces [31–33] revealed a type-I band alignment with the conduction-band offset  $\Delta E_c \simeq 0.4$  eV. The present pump light at 1.5 eV would then give sufficient excess energy to the photoexcited carriers in Si, whose indirect band gap is 1.1 eV, to overcome the conduction-band offset and go into the GaP layer. To unambiguously determine the pathways will require further transient reflectivity experiments on the GaP/Si heterointerfaces with a tunable pump light source, which is beyond the scope of the present study.

## V. CONCLUSION

We investigated the carrier and phonon dynamics of the GaP/Si interfaces upon below-band-gap photoexcitation of GaP by means of pump-probe reflectivity measurements. We demonstrated the contribution of a buried Si substrate to the transient reflectivity signal, whether it is of electronic or phononic origin, to exhibit an oscillatory dependence on the thickness of an optically transparent GaP overlayer. The behavior was mainly due to the interference of the probe light reflected at the heterointerface, whereas the interference effect

on the pump intensity penetrating into the Si substrate was found to be minor in the present case. Based on this finding, we extracted the carrier-induced transient reflectivity arising from the heterointerface, which was found to be qualitatively different between the GaP nucleation layer and the overgrown layers. The knowledge obtained in the present study can also be applied to the quantitative analyses of transient reflectivity signals for wide varieties of buried semiconductor heterointerfaces.

### ACKNOWLEDGMENTS

We gratefully acknowledge funding by the Deutsche Forschungsgemeinschaft (DFG, German Research Foundation), Project-ID 223848855-SFB 1083. C.J.S. was partially supported by the Air Force Office of Scientific Research under Award No. FA9550-17-1-0341.

### APPENDIX A: COHERENT PHONON GENERATION AND DETECTION IN BULK SI AND GAP

Illumination with a femtosecond laser pulse can induce coherent optical phonons in semiconductors. The equation of motion of coherent phonons can be expressed by

$$\mu \left[ \frac{\partial^2 Q(t)}{\partial t^2} + 2\gamma_{\text{ph}} \frac{\partial Q(t)}{\partial t} + \omega_{\text{ph}}^2 Q(t) \right] = F(t) \quad (\text{A1})$$

with  $\mu$ ,  $Q$ ,  $\gamma_{\text{ph}}$ , and  $\omega_{\text{ph}}$  denoting the reduced mass, displacement, dephasing rate, and frequency of the phonon. For the coherent phonons to be efficiently generated, the rise time of the driving force  $F(t)$  should be equivalent to half the phonon period  $(2\omega_{\text{ph}})^{-1}$  or shorter.

The generation mechanism of the coherent phonons depends on the semiconductor and the excitation laser pulse. When the laser photon energy is below the fundamental band gap, impulsive stimulated Raman scattering (ISRS) [34] is the only known generation mechanism. In ISRS, a broadband femtosecond optical pulse offers multiple pairs of photons required for the stimulated process. The driving force  $F$  depends on the polarization of the optical electric field  $E$  through a third-rank Raman tensor  $\mathfrak{R}_{jkl} \equiv (\partial\chi/\partial Q)_{jkl}$  [3]:

$$F_j^{\text{ISRS}}(t) = \mathfrak{R}_{jkl} E_k(t) E_l(t), \quad (\text{A2})$$

where  $j, k, l$  denote the Cartesian coordinates. The Raman tensor of diamond- and zinc-blende-structured crystals is given in the form of [1]

$$\begin{aligned} \mathfrak{R}_{xkl} &= \begin{pmatrix} 0 & 0 & 0 \\ 0 & 0 & a \\ 0 & a & 0 \end{pmatrix}, \quad \mathfrak{R}_{ykl} = \begin{pmatrix} 0 & 0 & a \\ 0 & 0 & 0 \\ a & 0 & 0 \end{pmatrix}, \\ \mathfrak{R}_{zkl} &= \begin{pmatrix} 0 & a & 0 \\ a & 0 & 0 \\ 0 & 0 & 0 \end{pmatrix}. \end{aligned} \quad (\text{A3})$$

In the backreflection from the (001)-oriented surface, in which the pump light polarization has no  $z$  component, the driving force can be reduced to

$$\begin{aligned} F_z^{\text{ISRS}}(t) &= \mathfrak{R}_{zxy} E_x(t) E_y(t) + \mathfrak{R}_{zyx} E_y(t) E_x(t) \\ &= a|E(t)|^2 \sin 2\theta' = a|E(t)|^2 \cos 2\theta, \end{aligned} \quad (\text{A4})$$

with  $E_x \equiv |E| \cos \theta'$ ,  $E_y \equiv |E| \sin \theta'$ , and  $\theta' \equiv \theta - \pi/4$  being the polarization angle from the [100] axis. The driving force becomes maximum at  $\theta = 0$  or  $\pi$ , i.e., when the pump light is polarized along the [110] or  $[-110]$  axis of the crystal. The direction of the driving force reverses between these two polarizations, which explains the phase flip of the coherent LO phonons of bulk GaP and Si shown in Fig. 2(b).

When the photon energy exceeds the band gap, the ISRS generation of coherent phonons can be resonantly enhanced in a similar manner as in spontaneous Raman scattering [35,36]. In the case of a polar semiconductor such as GaP, transient depletion field screening (TDFS) can contribute in addition [3,24]. In the TDFS mechanism, separation of photoexcited electrons and holes in the surface depletion region induces ultrafast drift-diffusion current  $J_z$  in the surface normal direction and thereby offers a driving force for the coherent polar phonons [3]:

$$F_z^{\text{TDFS}}(t) = -\frac{e^*}{\varepsilon_{\infty} \varepsilon_0} \int_{-\infty}^t dt' J_z(t'). \quad (\text{A5})$$

In a cubic crystal whose optical absorption is isotropic within the {001} plane, the driving force is independent of the pump polarization.

The coherent phonons can be observed as a periodic modulation of reflectivity at the zone-center optical phonon frequency. A nuclear displacement  $Q$  associated with the LO phonon oscillation induces a change in reflectivity  $R$  through the refractive index  $n$  and the susceptibility  $\chi$ . In a first-order approximation, the change  $\Delta R$  is given by [3]

$$\Delta R = \frac{\partial R}{\partial n} \Delta n \simeq \frac{\partial R}{\partial \chi} \frac{\partial \chi}{\partial Q} \Delta Q. \quad (\text{A6})$$

Here  $\partial\chi/\partial Q = \mathfrak{R}$  is the first-order Raman tensor given in Eq. (A3). Equation (A6) implies that only Raman-active phonons can be detected in transient reflectivity, and that the phonon signal depends on the probe light polarization angle  $\theta$  in the same manner as the pump light described in Eq. (A4).

### APPENDIX B: ESTIMATION OF TWO-PHOTON ABSORPTION

An ultrafast laser pulse can excite free carriers in a semiconductor if the photon energy  $\hbar\omega$  is above the band gap. If the photon energy is below the band gap, carriers can still be excited in the high irradiance region near the beam focus by simultaneous absorption of two photons. The carrier generation in the semiconductor can be expressed by [37]

$$\frac{dN(r, z)}{dz} = \frac{\alpha I(r, z)}{\hbar\omega} + \frac{\beta I^2(r, z)}{2\hbar\omega}, \quad (\text{B1})$$

where  $N$  and  $I$  are the free-carrier density and the pulse irradiance.  $\alpha$  and  $\beta$  represent the linear absorption coefficient and the two-photon absorption (TPA) coefficient. When TPA is the only absorption mechanism in the material, the photo-generated carrier density can be expressed by

$$N_{2\text{P}} = \frac{\beta}{2\hbar\omega} \int_{-\infty}^{\infty} I^2(z, t) dt. \quad (\text{B2})$$

In the experiments reported in Sec. III A, we use a pump pulse with a duration  $\Delta\tau = 12$  fs at a typical incident fluence

$F = 0.18 \text{ mJ/cm}^2/\text{pulse}$ . The corresponding peak power density is  $I \simeq (1 - R)F/\Delta\tau \simeq 11 \text{ GW/cm}^2$ . Using a previously reported TPA coefficient of GaP,  $\beta = 1 \text{ cm/GW}$  [38], we approximately obtain

$$N_{2P} \simeq \frac{\beta}{2\hbar\omega} I^2 \Delta\tau = 1.2 \times 10^{16} \text{ cm}^{-3}. \quad (\text{B3})$$

In the experiments reported in Sec. III B, in which we use  $\Delta\tau = 150 \text{ fs}$ ,  $F = 0.25 \text{ mJ/cm}^2/\text{pulse}$ , the peak power density is  $I \simeq (1 - R)F/\Delta\tau \simeq 1.2 \text{ GW/cm}^2$ . The corresponding carrier density created via two-photon absorption would be

$$N_{2P}(z) \simeq 4.4 \times 10^{14} \text{ cm}^{-3}. \quad (\text{B4})$$

We now evaluate the reflectivity change that would be induced by the carrier density obtained above. At a surface of a semiconductor whose refractive index is  $n$ , the intensity of the reflected probe light is expressed by  $R \equiv rr^*$  in the absence of the pump light, where  $r \equiv (1 - n)/(1 + n)$  is the reflection coefficient for the light wave. We assume that photoexcited carriers in the semiconductor induce a small disturbance  $\delta n$  in the refractive index. The pump-induced change in the reflected probe intensity can then be expressed by [39,40]

$$\frac{\Delta R}{R} = 2 \text{Re} \left( \frac{\delta r}{r} \right) = -\frac{4\delta n}{1 - n^2}. \quad (\text{B5})$$

The refractive index can be related to the dielectric constant,  $n^2 \equiv \epsilon$ , and the carrier-induced change can be expressed accordingly by

$$2n\delta n = \delta\epsilon. \quad (\text{B6})$$

On the basis of the Drude model, the dielectric function at the laser frequency  $\omega_L$  can be expressed by [1]

$$\epsilon(\omega_L) = \epsilon_\infty - \frac{Ne^2}{\epsilon_0 m^* (\omega_L^2 + i\omega_L\gamma)}, \quad (\text{B7})$$

with  $N$ ,  $e$ ,  $m^*$ , and  $\gamma$  being the density, charge, effective mass, and the scattering rate of the free carriers. Typically, the laser frequency is such that  $\gamma \ll \omega_L$ . This leads to a carrier-induced change in the dielectric constant:

$$\delta\epsilon \simeq -\frac{e^2}{\epsilon_0 m^* \omega_L^2} \delta N. \quad (\text{B8})$$

From Eqs. (B5), (B6), and (B8), we obtain

$$\frac{\Delta R}{R} = \frac{2}{n(1 - n^2)} \frac{e^2}{\epsilon_0 m^* \omega_L^2} \delta N. \quad (\text{B9})$$

Here, the effective mass  $m^*$  we use is that for the mixed, two-component plasma  $m_{eh} = 0.22m_e$  obtained from

$$m_{eh}^{-1} = m_X^{-1} + m_{\text{HH}}^{-1}, \quad (\text{B10})$$

where  $m_{\text{HH}}$  and  $m_X$  are, respectively, the mass of the heavy hole and the optical effective mass for the  $X$  valley electron. The  $X$  valley optical mass is given by  $m_X^{-1} = (2/3)m_r^{-1} + (1/3)m_l^{-1}$  [24]. Using  $n = 3.02$  at  $\hbar\omega_L = 1.55 \text{ eV}$  for GaP, we obtain

$$\frac{\Delta R}{R} = 2.2 \times 10^{-22} \delta N', \quad (\text{B11})$$

where the change in carrier density  $\delta N'$  is given in units of  $\text{cm}^{-3}$ . For the TPA carrier densities estimated in Eqs. (B3) and (B4), we would obtain the reflectivity change in the order of  $\Delta R/R_0 \sim 10^{-6}$  and  $10^{-8}$ , respectively.

### APPENDIX C: REFLECTION AND TRANSMISSION OF LIGHT AT A HETEROINTERFACE

In this Appendix, we consider the transmission and reflection of light at a GaP/Si heterointerface, which consists of a GaP layer of thickness  $d$  on top of a semi-infinitely thick Si substrate, as schematically illustrated in Fig. 8. We assume that a light pulse, whose electric field in air is expressed by

$$E_i(z, t) = \tilde{E}_i(z, t) e^{i(k_0 z - \omega_0 t)}, \quad (\text{C1})$$

is incident from the normal direction. Here  $\tilde{E}_i(z, t)$  and  $\exp[i(k_0 z - \omega_0 t)]$  represent the slowly varying envelope function and the fast varying carrier wave.  $z$  and  $t$  represent the distance from the air/GaP interface and time.  $\omega_0$  and  $k_0 = \omega_0/c$  denote the light wave frequency and the wave vector. Hereafter, we approximate the slowly varying envelope function in Eq. (C1) as a time-independent constant.

At the air/GaP interface at  $z = 0$ , the light pulse is partially reflected and partially transmitted into the GaP layer. The reflected and transmitted light waves can be expressed by

$$\begin{aligned} E_{1r}(z, t) &= \tilde{E}_{1r}(z, t) e^{-i(k_0 z + \omega_0 t)}, \\ E_{1t}(z, t) &= \tilde{E}_{1t}(z, t) e^{i(\tilde{n}_1 k_0 z - \omega_0 t)}, \end{aligned} \quad (\text{C2})$$

where  $\tilde{n}_1 = n_1 + ik_1$  is the refractive index of GaP. We use  $n_1 = 3.18$  and  $\kappa_1 = 0$  at wavelength  $\lambda_0 = 2\pi/k_0 = 815 \text{ nm}$  [26] in the following calculations. We apply the boundary condition that the in-plane components of the electric and magnetic fields are continuous, and we obtain the reflection and transmission coefficients for the light wave incoming from air into GaP:

$$\begin{aligned} r_{01} &\equiv \frac{\tilde{E}_{1r}}{\tilde{E}_i} = \frac{1 - n_1}{1 + n_1} = -0.52, \\ t_{01} &\equiv \frac{\tilde{E}_{1t}}{\tilde{E}_i} = \frac{2}{1 + n_1} = 0.48. \end{aligned} \quad (\text{C3})$$

The light wave transmitted into the GaP layer is again partially reflected at the GaP/Si interface and partially transmitted into the Si substrate. We describe the reflected and transmitted waves by

$$\begin{aligned} E_{2r}(z, t) &= \tilde{E}_{2r}(z, t) e^{-i[n_1 k_0(z - 2d) + \omega_0 t]}, \\ E_{2t}(z, t) &= \tilde{E}_{2t}(z, t) e^{i[\tilde{n}_2 k_0 d + \tilde{n}_2 k_0(z - d) - \omega_0 t]}, \end{aligned} \quad (\text{C4})$$

where  $\tilde{n}_2 = n_2 + ik_2$  is the refractive index of Si, with  $n_2 = 3.68$  and  $\kappa_2 = 0.006$  at  $\lambda_0 = 815 \text{ nm}$  [26]. Equation (C4) implies that the light wave gains a thickness-dependent phase shift,  $\phi \equiv n_1 k_0 d$ , while it crosses the GaP layer once. We apply the boundary condition at the GaP/Si interface and obtain the reflection and transmission coefficients for the light

wave incoming from GaP into Si:

$$\begin{aligned} r_{12} &= \frac{\tilde{E}_{2r}}{\tilde{E}_{1r}} = \frac{n_1 - n_2}{n_1 + n_2} = -0.073, \\ t_{12} &= \frac{\tilde{E}_{2t}}{\tilde{E}_{1r}} = \frac{2n_1}{n_1 + n_2} = 0.93. \end{aligned} \quad (\text{C5})$$

Here we neglect the small optical absorption in Si and approximate  $\tilde{n}_2 \simeq n_2$ . After the reflection at the GaP/Si interface, the light wave is again partially reflected at the GaP/air interface and partially transmitted into air. We describe the reflected and transmitted waves by

$$\begin{aligned} E_{3r}(z, t) &= \tilde{E}_{3r}(z, t)e^{i(\tilde{n}_1 k_0 z - \omega_0 t + 2\phi)}, \\ E_{3t}(z, t) &= \tilde{E}_{3t}(z, t)e^{-i(k_0 z + \omega_0 t + 2\phi)}. \end{aligned} \quad (\text{C6})$$

We apply the similar boundary condition and obtain the reflection and transmission coefficients for an outgoing wave from GaP into air:

$$\begin{aligned} r_{10} &= \frac{\tilde{E}_{3r}}{\tilde{E}_{2r}} = \frac{n_1 - 1}{n_1 + 1} = 0.52, \\ t_{10} &= \frac{\tilde{E}_{3t}}{\tilde{E}_{2r}} = \frac{2n_1}{n_1 + 1} = 1.52. \end{aligned} \quad (\text{C7})$$

The amplitude ratio  $r_0$  of the outgoing wave into air to the incident wave can be given by the sum of multiple reflection pathways:

$$\begin{aligned} r_0 &\equiv \frac{\tilde{E}_{1r} + \tilde{E}_{3r}e^{2i\phi} + \tilde{E}_{5r}e^{4i\phi} + \tilde{E}_{7r}e^{6i\phi} + \dots}{\tilde{E}_i} \\ &= r_{01} + t_{01}r_{12}t_{10}e^{2i\phi}(1 + r_{10}r_{12}e^{2i\phi} + r_{10}^2r_{12}^2e^{4i\phi} + \dots) \\ &= r_{01} + \frac{t_{01}r_{12}t_{10}e^{2i\phi}}{1 - r_{10}r_{12}e^{2i\phi}} = \frac{r_{01} + r_{12}e^{2i\phi}}{1 + r_{01}r_{12}e^{2i\phi}}. \end{aligned} \quad (\text{C8})$$

Here we use the relations  $t_{01}t_{10} = 1 + r_{10}r_{01}$  and  $r_{10} = -r_{01}$  derived from Eqs. (C3) and (C7). Likewise, the amplitude ratio  $t_0$  of the incoming wave into Si to the incident wave can be given by

$$\begin{aligned} t_0 &\equiv \frac{\tilde{E}_{2t}e^{i\phi} + \tilde{E}_{4t}e^{3i\phi} + \tilde{E}_{6t}e^{5i\phi} + \dots}{\tilde{E}_i} \\ &= t_{01}t_{12}e^{i\phi}(1 + r_{10}r_{12}e^{2i\phi} + r_{10}^2r_{12}^2e^{4i\phi} + \dots) \\ &= \frac{t_{01}t_{12}e^{i\phi}}{1 - r_{10}r_{12}e^{2i\phi}}. \end{aligned} \quad (\text{C9})$$

The reflectance, or the light *intensity* reflected into air, can then be given by

$$\begin{aligned} R_0 &= |r_0|^2 = \frac{|r_{01} + r_{12}e^{2i\phi}|^2}{|1 + r_{01}r_{12}e^{2i\phi}|^2} \\ &= \frac{r_{01}^2 + r_{12}^2 + 2r_{01}r_{12}\cos 2\phi}{1 + r_{01}^2r_{12}^2 + 2r_{01}r_{12}\cos 2\phi}. \end{aligned} \quad (\text{C10})$$

The transmittance, or the light intensity transmitted into the Si substrate, can be given by

$$\begin{aligned} T_0 &= 1 - R_0 \\ &= \frac{(1 - r_{01}^2)(1 - r_{12}^2)}{1 + r_{01}^2r_{12}^2 + 2r_{01}r_{12}\cos 2\phi}. \end{aligned} \quad (\text{C11})$$

The red dashed curve in Fig. 6(b) shows the transmittance given by Eq. (C11) as a function of the GaP thickness  $d$ . The calculation indicates that the pump intensity transmitted into Si is modified by no more than 15% with varying  $d$ , which is too small to explain the experimental  $d$ -dependences of  $B_{\text{Si}}$  plotted in the same figure.

#### APPENDIX D: PUMP-INDUCED CHANGES IN REFLECTIVITY FROM THE GaP/Si HETEROINTERFACE

In this Appendix, we consider the pump-induced change in the probe light wave reflected from the GaP/Si heterointerface. We assume that a pump wave induces small disturbances  $\delta n_1(z, t)$  and  $\delta n_2(z, t)$  in the refractive indices  $n_1$  and  $n_2$  in the GaP layer ( $0 < z < d$ ) and in the Si substrate ( $z > d$ ), respectively. Because the semiconductors have very small or no absorption to the pump light, we can approximate the disturbances to be independent of the depth  $z$  in both GaP and Si and to depend only on the time delay  $t$  between the pump and probe pulses. Coherent phonons in the respective semiconductors modulate  $n_1$  and  $n_2$  periodically as a function of  $t$ , whereas photoexcited carriers in Si induce a step-function-like change in  $n_2$ .

To determine the pump-induced change in the reflectance, we can take derivatives of the reflectance with respect to the refractive indices:

$$\frac{\Delta R}{R_0} = \frac{1}{R_0} \left( \frac{\partial R_0}{\partial n_1} \delta n_1 + \frac{\partial R_0}{\partial n_2} \delta n_2 \right). \quad (\text{D1})$$

A change in  $n_1$  can modify  $r_{01}$ ,  $r_{12}$ , and  $\phi = n_1 k_0 d$ , whereas a change in  $n_2$  can affect only  $r_{12}$ . The first and second terms of Eq. (D1) can therefore be expressed by

$$\begin{aligned} \frac{1}{R_0} \frac{\partial R_0}{\partial n_1} \delta n_1 &= \frac{1}{R_0} \left( \frac{\partial R_0}{\partial r_{01}} \frac{\partial r_{01}}{\partial n_1} + \frac{\partial R_0}{\partial r_{12}} \frac{\partial r_{12}}{\partial n_1} + \frac{\partial R_0}{\partial \phi} \frac{\partial \phi}{\partial n_1} \right) \delta n_1 \\ &= \frac{2(r_{01}^2 - 1)(1 - r_{12}^2)}{(r_{01}^2 + r_{12}^2 + 2r_{01}r_{12}\cos 2\phi)(1 + r_{01}^2r_{12}^2 + 2r_{01}r_{12}\cos 2\phi)} \\ &\quad \times \left[ \frac{r_{01}(1 + r_{12}^2) - r_{12}(1 + r_{01}^2)}{2n_1} (1 - \cos 2\phi) + 2k_0 d r_{01}r_{12} \sin 2\phi \right] \delta n_1 \equiv P_1(d) \delta n_1, \end{aligned} \quad (\text{D2})$$

$$\begin{aligned} \frac{1}{R_0} \frac{\partial R_0}{\partial n_2} \delta n_2 &= \frac{1}{R_0} \frac{\partial R_0}{\partial r_{12}} \frac{\partial r_{12}}{\partial n_2} \delta n_2 \\ &= \frac{2r_{12}(1 - r_{01}^4) + 2r_{01}(1 + r_{12}^2)(1 - r_{01}^2)\cos 2\phi}{(r_{01}^2 + r_{12}^2 + 2r_{01}r_{12}\cos 2\phi)(1 + r_{01}^2r_{12}^2 + 2r_{01}r_{12}\cos 2\phi)} \times \frac{-2n_1}{(n_1 + n_2)^2} \delta n_2 \equiv P_2(d) \delta n_2. \end{aligned} \quad (\text{D3})$$

Here we use

$$\frac{\partial R_0}{\partial r_{01}} = \frac{2r_{01}(1 - r_{12}^4) + 2r_{12}(r_{01}^2 + 1)(1 - r_{12}^2) \cos 2\phi}{(1 + r_{01}^2 r_{12}^2 + 2r_{01} r_{12} \cos 2\phi)^2}, \quad (\text{D4})$$

$$\frac{\partial R_0}{\partial r_{12}} = \frac{2r_{12}(1 - r_{01}^4) + 2r_{01}(1 + r_{12}^2)(1 - r_{01}^2) \cos 2\phi}{(1 + r_{01}^2 r_{12}^2 + 2r_{01} r_{12} \cos 2\phi)^2}. \quad (\text{D5})$$

$$\frac{\partial R_0}{\partial \phi} = \frac{-4r_{01} r_{12} (1 - r_{01}^2)(1 - r_{12}^2) \sin 2\phi}{(1 + r_{01}^2 r_{12}^2 + 2r_{01} r_{12} \cos 2\phi)^2}, \quad (\text{D6})$$

$$\frac{\partial r_{01}}{\partial n_1} = \frac{-2}{(1 + n_1)^2} = \frac{r_{01}^2 - 1}{2n_1}, \quad (\text{D7})$$

$$\frac{\partial r_{12}}{\partial n_1} = \frac{2n_2}{(n_1 + n_2)^2} = \frac{1 - r_{12}^2}{2n_1}, \quad (\text{D8})$$

$$\frac{\partial \phi}{\partial n_1} = k_0 d, \quad (\text{D9})$$

$$\frac{\partial r_{12}}{\partial n_2} = \frac{-2n_1}{(n_1 + n_2)^2} = \frac{r_{12}^2 - 1}{2n_1}. \quad (\text{D10})$$

Equations (D2) and (D3) reproduce the experimental  $d$ -dependences of the phonon-induced reflectivity signals from GaP and Si, as shown in Fig. 6.

- 
- [1] P. Y. Yu and M. Cardona, *Fundamentals of Semiconductors*, 3rd ed. (Springer, Berlin, 2005).
- [2] J. Sjakste, K. Tanimura, G. Barbarino, L. Perfetti, and N. Vast, *J. Phys.: Condens. Matter* **30**, 353001 (2018).
- [3] T. Dekorsy, G. Cho, and H. Kurz, Coherent phonons in condensed media, in *Light Scattering in Solids VIII*, Topics in Applied Physics, edited by M. Cardona and G. Güntherodt (Springer, Berlin, 2000), Vol. 76, p. 169.
- [4] O. Matsuda, M. C. Larciprete, R. Li Voti, and O. B. Wright, *Ultrasonics* **56**, 3 (2015).
- [5] Y. D. Glinka, N. H. Tolk, X. Liu, Y. Sasaki, and J. K. Furdyna, *J. Appl. Phys.* **103**, 043708 (2008).
- [6] T. Dekorsy, A. M. T. Kim, G. C. Cho, H. Kurz, A. V. Kuznetsov, and A. Förster, *Phys. Rev. B* **53**, 1531 (1996).
- [7] K. J. Yee, D. S. Yee, D. S. Kim, T. Dekorsy, G. C. Cho, and Y. S. Lim, *Phys. Rev. B* **60**, R8513(R) (1999).
- [8] M. Först and T. Dekorsy, Coherent phonons in bulk and low-dimensional semiconductors, in *Coherent Vibrational Dynamics*, Practical Spectroscopy, edited by S. D. Silvestri, G. Cerullo, and G. Lanzani (CRC, Boca Raton, FL, 2007), pp. 130–172.
- [9] P. Castrillo, G. Armelles, J. P. Silveira, F. Briones, and J. Barbolla, *Appl. Phys. Lett.* **71**, 1353 (1997).
- [10] J. Gleize, F. Demangeot, J. Frandon, M. A. Renucci, F. Widmann, and B. Daudin, *Appl. Phys. Lett.* **74**, 703 (1999).
- [11] H. Jeong, Y. D. Jho, S. H. Rhim, K. J. Yee, S. Y. Yoon, J. P. Shim, D. S. Lee, J. W. Ju, J. H. Baek, and C. J. Stanton, *Phys. Rev. B* **94**, 024307 (2016).
- [12] T. N. Thanh, C. Robert, W. Guo, A. Letoublon, C. Cornet, G. Elias, A. Ponchet, T. Rohel, N. Bertru, A. Balocchi, O. Durand, J. S. Micha, M. Perrin, S. Loulaliche, X. Marie, and A. L. Corre, *J. Appl. Phys.* **112**, 053521 (2012).
- [13] A. C. Lin, M. M. Fejer, and J. S. Harris, *J. Cryst. Growth* **363**, 258 (2013).
- [14] K. Volz, A. Beyer, W. Witte, J. Ohlmann, I. Nemeth, B. Kunert, and W. Stolz, *J. Cryst. Growth* **315**, 37 (2011).
- [15] A. Beyer, I. Nemeth, S. Liebich, J. Ohlmann, W. Stolz, and K. Volz, *J. Appl. Phys.* **109**, 083529 (2011).
- [16] A. Beyer, J. Ohlmann, S. Liebich, H. Heim, G. Witte, W. Stolz, and K. Volz, *J. Appl. Phys.* **111**, 083534 (2012).
- [17] A. Beyer, A. Stegmüller, J. O. Oelerich, K. Jandieri, K. Werner, G. Mette, W. Stolz, S. D. Baranovskii, R. Tonner, and K. Volz, *Chem. Mater.* **28**, 3265 (2016).
- [18] J. Belz, A. Beyer, and K. Volz, *Micron* **114**, 32 (2018).
- [19] A. Beyer and K. Volz, *Adv. Mater. Interfaces* **6**, 1801951 (2019).
- [20] K. Ishioka, K. Brixius, A. Beyer, A. Rustagi, C. J. Stanton, W. Stolz, K. Volz, U. Höfer, and H. Petek, *Appl. Phys. Lett.* **108**, 051607 (2016).
- [21] K. Ishioka, A. Rustagi, A. Beyer, W. Stolz, K. Volz, U. Höfer, H. Petek, and C. J. Stanton, *Appl. Phys. Lett.* **111**, 062105 (2017).
- [22] K. Ishioka, A. Beyer, W. Stolz, K. Volz, P. Hrvoje, U. Höfer, and C. J. Stanton, *J. Phys.: Condens. Matter* **31**, 094003 (2019).
- [23] M. Hase, M. Kitajima, A. Constantinescu, and H. Petek, *Nature (London)* **426**, 51 (2003).
- [24] K. Ishioka, K. Brixius, U. Höfer, A. Rustagi, E. M. Thatcher, C. J. Stanton, and H. Petek, *Phys. Rev. B* **92**, 205203 (2015).
- [25] G. Mette, J. E. Zimmermann, A. Lerch, K. Brixius, J. Güdde, A. Beyer, M. Dürr, K. Volz, W. Stolz, and U. Höfer, *Appl. Phys. Lett.* **117**, 081602 (2020).
- [26] D. E. Aspnes and A. A. Studna, *Phys. Rev. B* **27**, 985 (1983).
- [27] The oscillations shown in Fig. 2 also include a low-frequency modulation at 2 THz, which is especially evident for the pump polarization labeled with I. This modulation is seen only for the GaP/Si samples and absent for the bulk GaP and Si. We tentatively attribute this modulation to a phonon mode localized at the GaP/Si interface, and we will report further results in a separate publication.
- [28] Experimental carrier-induced transient reflectivity signal,  $\Delta R/R_0$ , is expected to be at least several times larger than  $\Delta R_{\text{eo}}/R_0$  plotted in Fig. 2(a), since the isotropic component of the signal is canceled in the latter.
- [29] A. J. Sabbah and D. M. Riffe, *J. Appl. Phys.* **88**, 6954 (2000).
- [30] A. J. Sabbah and D. M. Riffe, *Phys. Rev. B* **66**, 165217 (2002).
- [31] R. G. Dandrea, S. Froyen, and A. Zunger, *Phys. Rev. B* **42**, 3213 (1990).
- [32] P. Perfetti, F. Patella, F. Sette, C. Quaresima, C. Capasso, A. Savoia, and G. Margaritondo, *Phys. Rev. B* **30**, 4533 (1984).
- [33] I. Sakata and H. Kawanami, *Appl. Phys. Express* **1**, 091201 (2008).

- [34] L. Dhar, J. Rogers, and K. Nelson, *Chem. Rev.* **94**, 157 (1994).
- [35] T. E. Stevens, J. Kuhl, and R. Merlin, *Phys. Rev. B* **65**, 144304 (2002).
- [36] M. Cardona, Resonance phenomena, in *Light Scattering in Solids II*, edited by M. Cardona and G. Güntherodt (Springer, Berlin, 1982), Book Sec.2, p. 19.
- [37] D. McMorrow, W. T. Lotshaw, J. S. Melinger, S. Buchner, and R. L. Pease, *IEEE Trans. Nucl. Sci.* **49**, 3002 (2002).
- [38] R. C. Hoffman and A. G. Mott, Measurement of the two-photon absorption coefficient of gallium phosphide (GaP) using a dispersion-minimized sub-10 femtosecond Z-scan measurement system, Army Research Laboratory Adelphi MD Sensors and Electron Devices Directorate, Report No. ARL-TR-6157 (2012).
- [39] R. Liu, G. D. Sanders, C. J. Stanton, C. S. Kim, J. S. Yahng, Y. D. Jho, K. J. Yee, E. Oh, and D. S. Kim, *Phys. Rev. B* **72**, 195335 (2005).
- [40] C. J. Cook, S. Khan, G. D. Sanders, X. Wang, D. H. Reitze, Y. D. Jho, Y.-W. Heo, J.-M. Erie, D. P. Norton, and C. J. Stanton, *Proc. SPIE* **7603**, 760304 (2010).